

Figure S1. Expression and functional analysis of the m³C writers in various tissues and pancreatic cancer. (A) qRT-PCR analysis of relative *METTL2B*, *METTL6*, and *METTL8* expression in AsPC-1 cells after siRNA-mediated knockdown (KD) with two independent siRNAs (#1 and #2). n = 3; Student's t-test (*: p < 0.05). (B) The viability of AsPC-1 cells transfected with siRNAs targeting *METTL2B*, *METTL6*, or *METTL8*, assessed by CellTiter-Glo assays. n = 3; Student's t-test. n.s.: not significant.

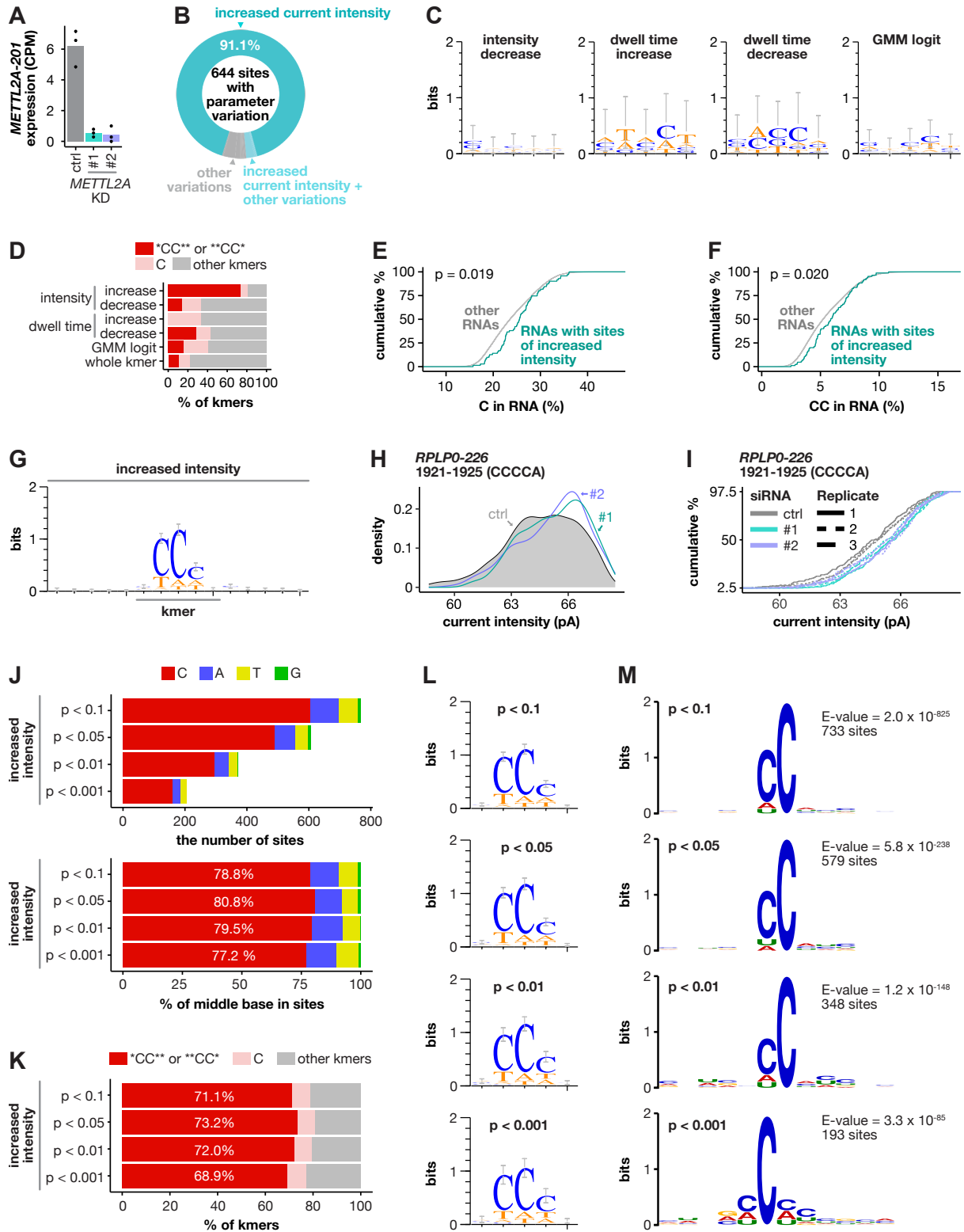


Figure S2. METTL2A-mediated m³C sites are enriched in the CC motif of poly(A) RNA. (A) Counts per million (CPM) values for *METTL2A* measured by nanopore direct RNA sequencing for each condition are shown. (B) Percentage of sites with increased current intensity and other parameter variations. (C) Logo plot of *k*-mer sequences enriched at the sites where signal alterations were consistently detected with both siRNAs. (D) Percentage of *k*-mer sequences with consecutive C bases in the middle position. (E, F) Cumulative percentage of the C (E) and CC (F) content in RNAs with and without sites of increased current intensity. Statistical significance was determined by Wilcoxon test. (G) Logo plot of sequences surrounding the sites with increased current intensity on *METTL2A* knockdown. (H) Distribution of current intensity at the indicated position in *RPLP0-226*, where increases were commonly detected with both siRNAs. The gray area represents the control condition, while the green and purple lines indicate *METTL2A* knockdown conditions. (I) Cumulative percentage of current intensity for each sample at the indicated site. (J) Nucleotide composition analysis of sites with increased intensity, categorized by different *p*-value cut-offs. Top chart shows the number of sites, while bottom chart shows the percentage of middle base composition. (K) *K*-mer composition of sites with increased intensity, showing the percentage of “CC” or “CC” *k*-mers (red), *k*-mers containing “C” (light red), and other *k*-mers (gray) across different *p*-value cut-offs. (L) WebLogo sequence logos for sites with increased intensity at different *p*-value cut-offs. (M) MEME motif analysis for sites with increased current intensity at different *p*-value cut-offs. No other statistically significant motifs were detected beyond the CC motif.

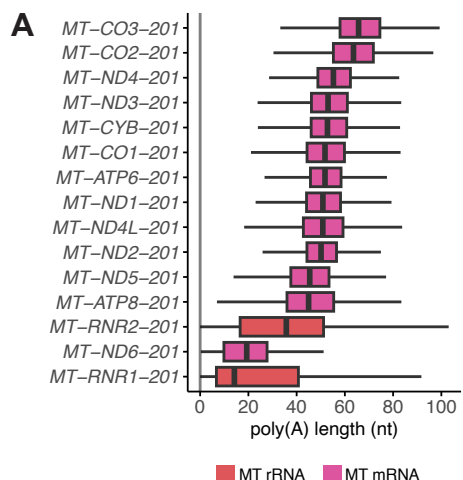


Figure S3. Poly(A) tail lengths of mitochondrial transcripts. (A) Boxplots showing the distribution of poly(A) tail lengths for individual mitochondrial transcripts across all samples.

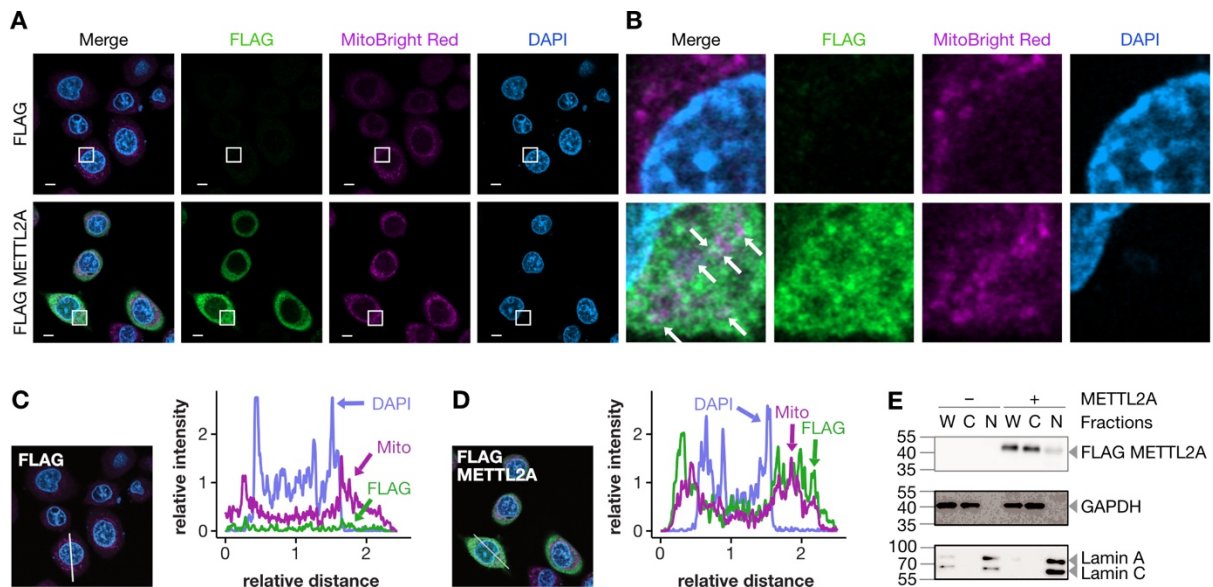


Figure S4. Subcellular localization of METTL2A in AsPC-1 cells. (A) Immunofluorescence analysis of AsPC-1 cells transfected with FLAG or FLAG-METTL2A. Cells were stained with anti-FLAG antibody (green), MitoBright Red (magenta) for mitochondria, and DAPI (blue) for nuclei. Merged images and individual channels are shown. Scale bars: 5 μ m. (B) Enlarged images of the boxed regions in (A), showing higher magnification of FLAG- and FLAG-METTL2A-expressing cells. Co-localization sites of FLAG-METTL2A with mitochondria are indicated by arrows. (C) Line-scan analysis of fluorescence intensity across the indicated line in FLAG-expressing cells shown in (A). The intensity profiles of FLAG (green), MitoBright Red (magenta), and DAPI (blue) are plotted. (D) Line-scan analysis of fluorescence intensity across the indicated line (A–B) in FLAG-METTL2A-expressing cells shown in (A). The intensity profiles of FLAG (green), MitoBright Red (magenta), and DAPI (blue) are plotted. (E) Subcellular fractionation and immunoblot analysis of AsPC-1 cells expressing FLAG or FLAG-METTL2A. Whole-cell lysate (W), and cytoplasmic (C) and nuclear (N) fractions were analyzed by immunoblotting with antibodies against FLAG, GAPDH (cytoplasmic marker), and Lamin A/C (nuclear marker).

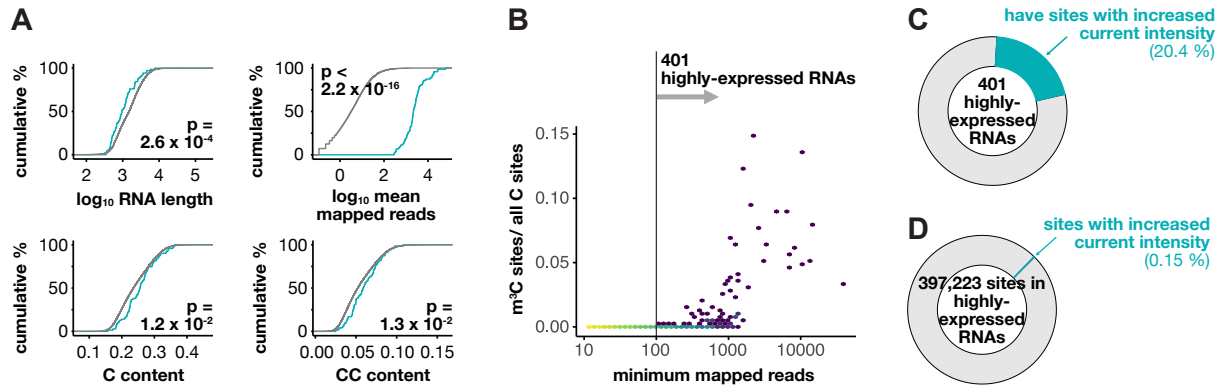


Figure S5. Selective detection of m^3C sites in highly expressed RNAs. (A) Cumulative percentage of RNA length, the mean number of mapped reads, C content, and CC content in m^3C RNAs versus other RNAs. Statistical significance was determined by Wilcoxon test. (B) Correlation between the minimum number of mapped reads per RNA and the fraction of C sites that are m^3C sites. (C) Percentage of highly expressed RNAs with sites of increased current intensity. (D) Percentage of sites with increased current intensity among all sites in highly expressed RNAs.

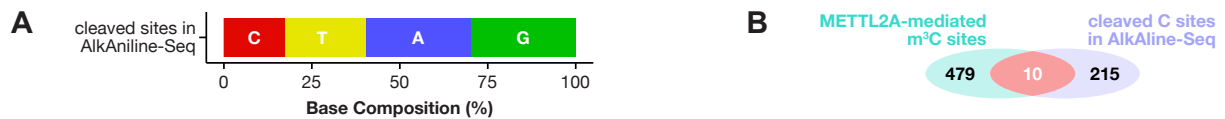
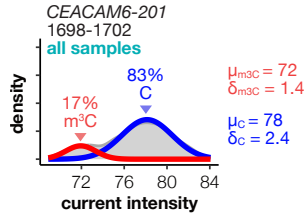


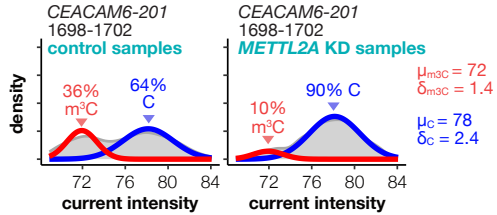
Figure S6. Characterization of cleaved sites in AlkAniline-Seq and overlap with METTL2A-mediated m³C sites identified in this study. (A) Base composition at cleaved sites identified by AlkAniline-Seq. The bar plot shows the percentage of each nucleotide (C, T, A, G) at these cleaved sites. (B) Venn diagram illustrating the overlap between METTL2A-mediated m³C sites and cleaved C sites identified by AlkAniline-Seq.

A**1. Determine the two distributions using data from all samples**

The parameters are shared across all samples

**2. Determine the mixing proportion for each sample**

The mixing proportions are different among samples

**B**

- up (5)
- others (70)
- down (414)

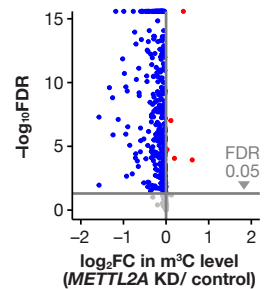


Figure S7. Estimation of stoichiometries at METTL2A-mediated m³C sites. (A) Two-step process for estimating m³C stoichiometry based on current intensity distributions. Step 1: Two normal distributions representing m³C (red) and unmodified cytosine (blue) were determined using data from all samples, with shared parameters across samples. Step 2: The mixing proportions of these distributions were estimated separately for control and METTL2A-knockdown (KD) samples. The example shows *CEACAM6*-201 positions 1698–1702, where control samples exhibited 36% m³C and 64% C, while *METTL2A* KD samples showed 10% m³C and 90% C. (B) Volcano plot of differential m³C modification levels upon *METTL2A* knockdown. Red circles indicate sites with increased m³C levels (5 sites), blue circles indicate sites with decreased m³C levels (414 sites). The horizontal line represents FDR = 0.05 threshold.

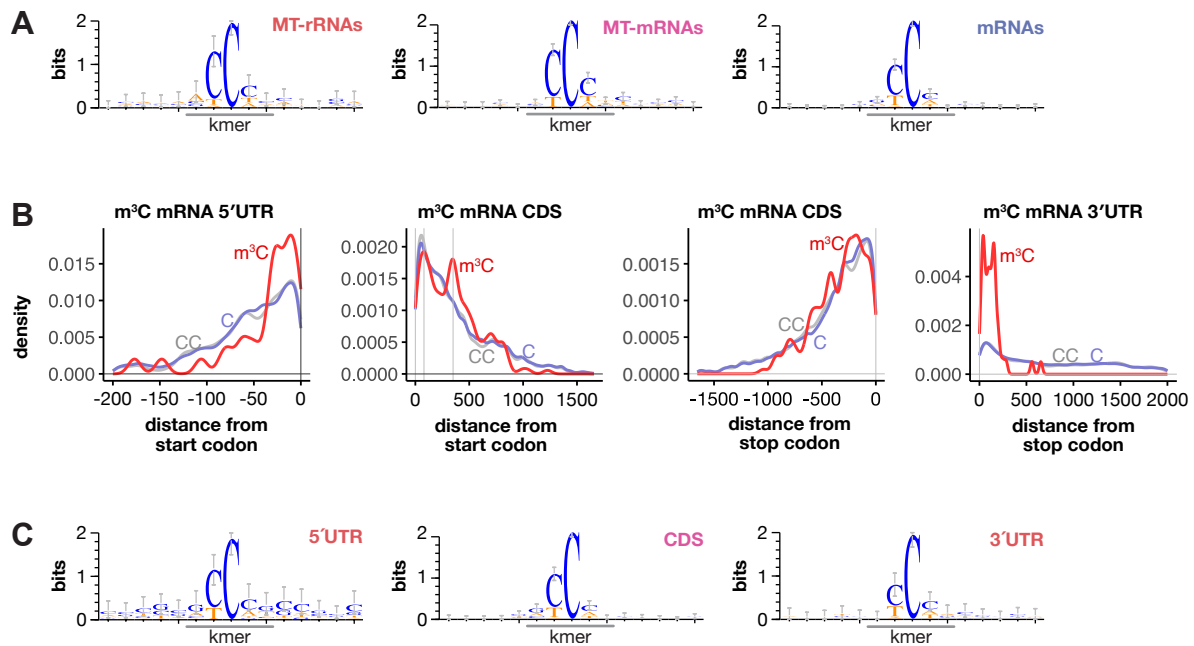


Figure S8. m³C sites are enriched in coding sequences. (A) Logo plots of the sequences near m³C sites within MT-rRNAs, MT-mRNAs, and mRNAs. (B) Distribution of m³C sites near the start or stop codon of mRNAs. (C) Logo plots of the sequences near m³C sites across different regions of the mRNAs.

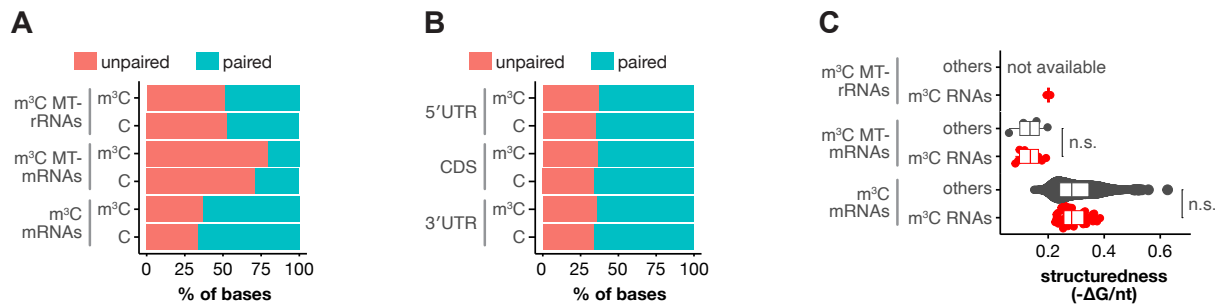


Figure S9. Structural context of METTL2A-mediated m³C sites in RNAs. (A) Proportion of m³C and other C bases located in unpaired (orange) or paired (cyan) regions in mitochondrial (MT) mRNAs and non-mitochondrial mRNAs. (B) Proportion of m³C and other C bases located in unpaired or paired regions within different transcript regions (5'UTR, CDS, 3'UTR) of mRNAs. (C) Comparison of overall RNA structural features (structureness, $-\Delta G/nt$) between m³C-containing RNAs and other RNAs in mitochondrial and non-mitochondrial mRNAs. No significant difference (n.s.) was observed.

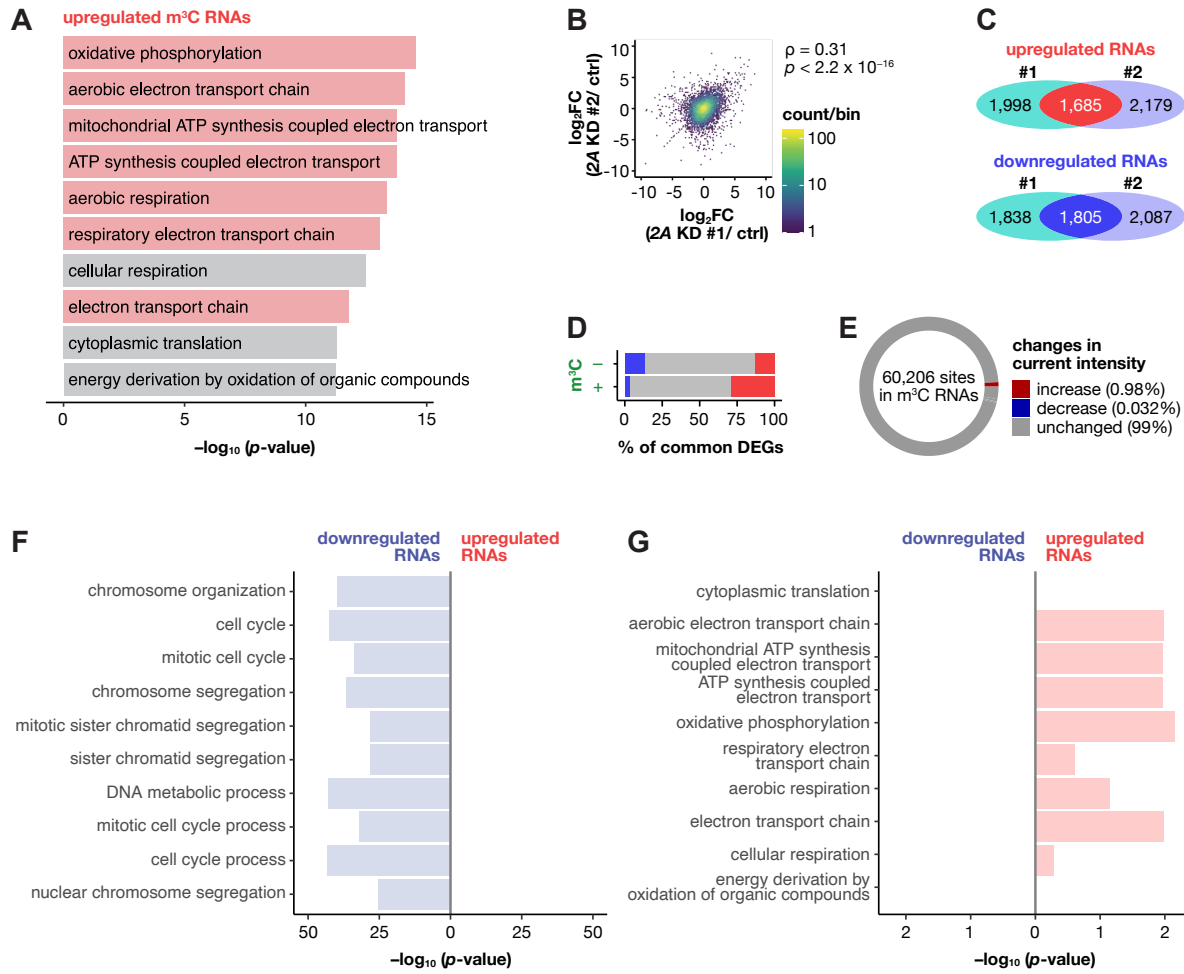


Figure S10. METTL2A downregulates m³C RNAs. (A) The top ten biological processes enriched in the 30 upregulated m³C RNAs. (B) Hexagonal two-dimensional heatmap showing the correlation of expression changes between the two siRNAs in the short-read RNA-seq data. Statistical significance was determined by Spearman's correlation test. 2A KD: METTL2A knockdown (C) Venn diagrams showing the number of transcripts that were upregulated and downregulated by each siRNA in the short-read RNA-seq data. (D) Stacked bar plots showing the percentage of m³C RNAs and other RNAs. (E) Donut chart summarizing the changes in current intensity at all positions in m³C RNAs upon METTL2A knockdown. (F, G) The biological processes associated with the downregulated and upregulated transcripts shown in Figure 5E within the upregulated (G) and downregulated (F) genes in the short-read RNA-seq. Enrichment in the upregulated and downregulated transcripts in genes is shown in red and blue, respectively.

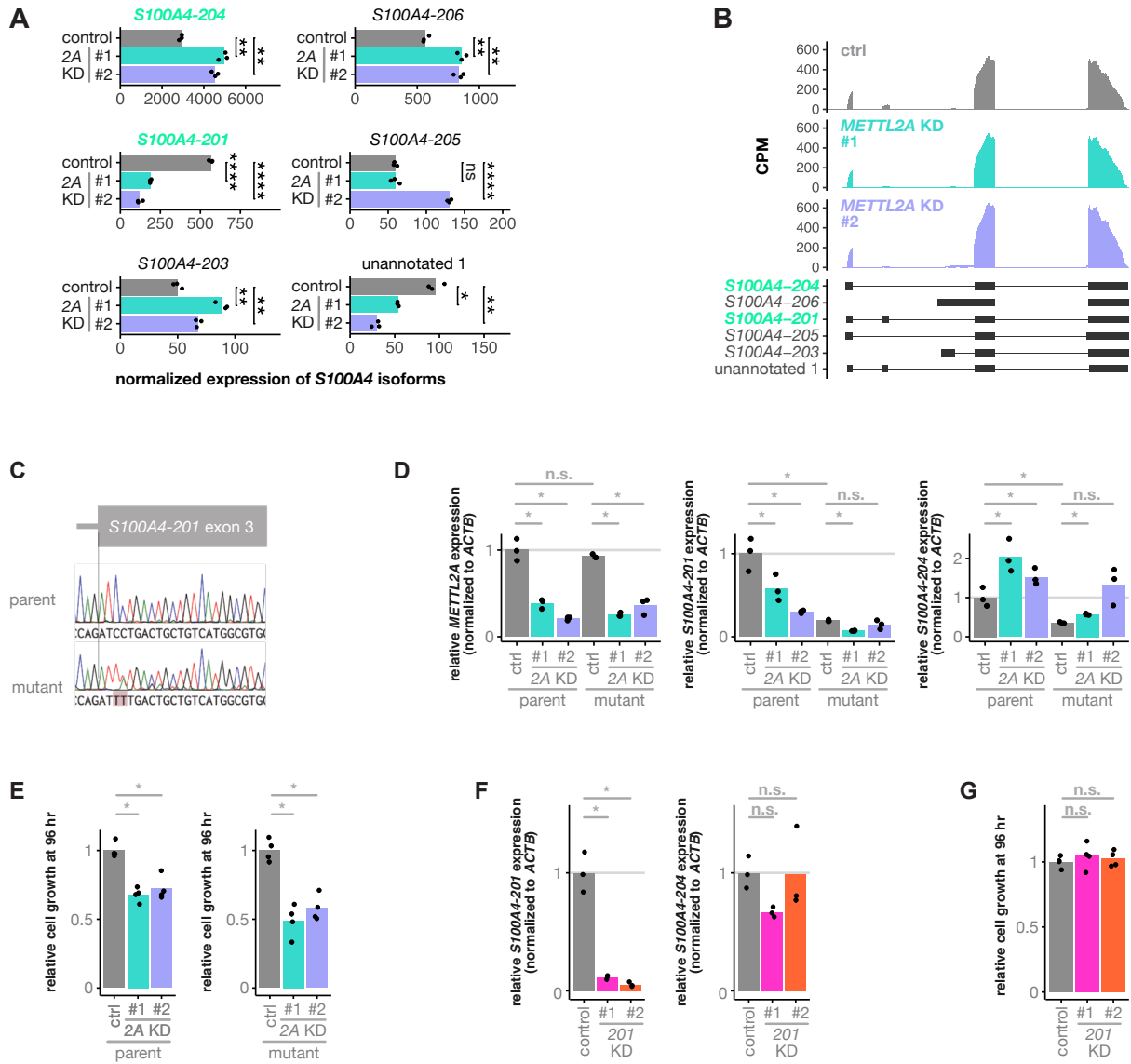


Figure S11. m^3C sites near exon junctions contribute to isoform usage in *S100A4* mRNA. (A) Bar plots showing the normalized expression of each *S100A4* isoform under each condition. (2A KD: *METTL2A* knockdown) (B) Short-read RNA sequencing mapping patterns of *S100A4* isoforms for each condition. Methylated isoforms are shown in green. Only isoforms representing more than 1% of total reads for the gene are shown. (C) Sanger sequencing chromatograms of the 5'-exon junction region of *S100A4-201* exon 3 in parental (top) and *S100A4* mutant (bottom) AsPC-1 cells. (D) Quantitative RT-PCR analysis of relative *METTL2A* (left), *S100A4-201* (middle), and *S100A4-204* (right) expression in parental and mutant AsPC-1 cells after *METTL2A* knockdown. n = 3. Student's t-test (*: p < 0.05, n.s.: not significant). (E) Relative cell growth at 96 h after *METTL2A* knockdown in parental (left) and *S100A4* mutant (right) AsPC-1 cells. n = 4. *: p < 0.05; n.s.: not significant. (F) Quantitative RT-PCR analysis of relative *S100A4-201* (left) and *S100A4-204* (right) expression in AsPC-1 cells after knockdown of *S100A4-201*. n = 3. Student's t-test (*: p < 0.05, n.s.: not significant). 201 KD: *S100A4-201* knockdown. (G) Relative cell growth at 96 h after *S100A4-201* knockdown in AsPC-1 cells. n = 4. n.s.: not significant.